

INTRODUCTION: 66055 has petrological characteristics intermediate between polymict fragmental breccias and dimict black and white rocks. Like dimict rocks the variety of lithic types within the broad dark and light divisions is restricted, and the clast-matrix relationships of dark and light are inconsistent. Like the fragmental breccias the lithologies are well-mixed on a small scale (Fig. 1) and include glass. The light material consists of fragments of anorthosite-noritic-troctolitic material and its degraded debris. The dark material varies from brown glass through fine-grained clast-rich breccia to mesostasis-rich impact basalt. Some white fragments are rimmed by dark material (Fig. 1).

66055 was collected from the north rim of a 10 m crater near the base of Stone Mountain. The sample is sub-angular, coherent, and has some penetrative fractures. It was only slightly buried and its orientation is known. The buried side had no zap pits and most occur on one side rather than the top.

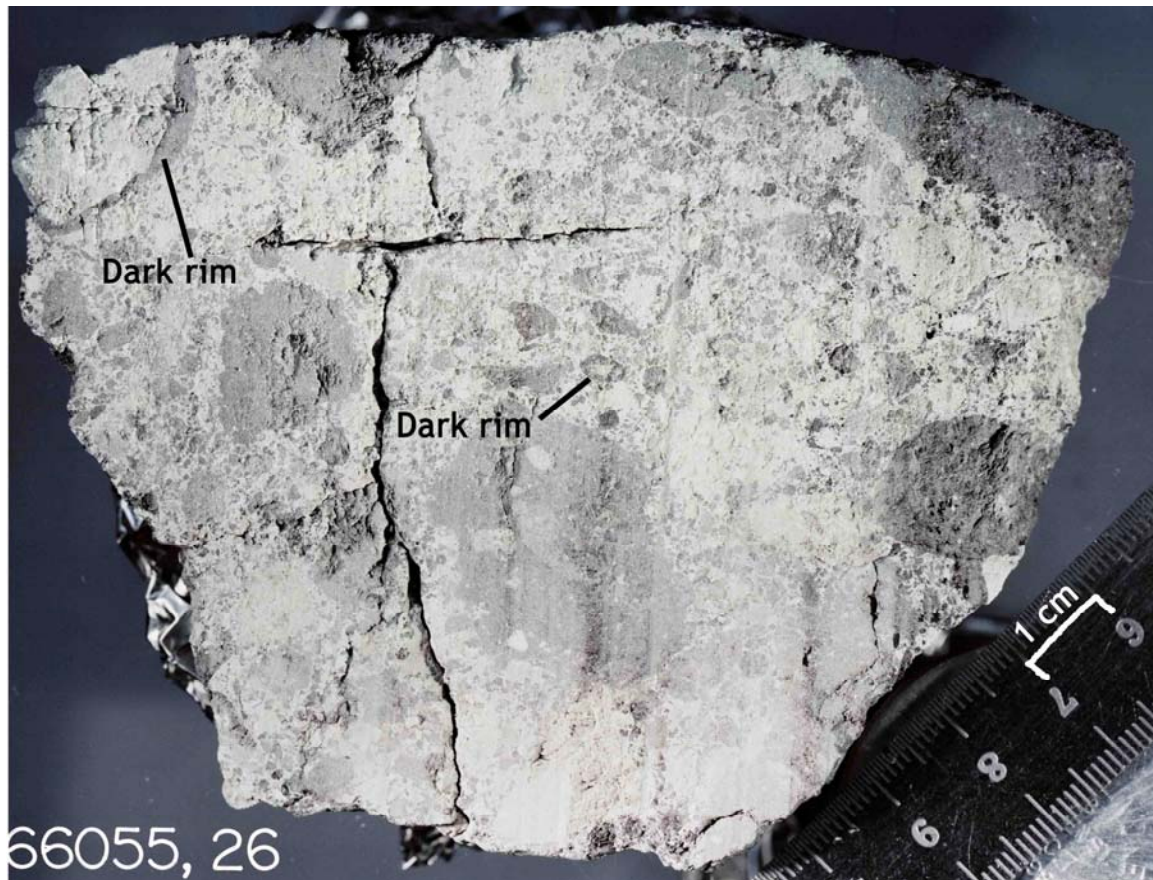


FIGURE 1. S-78-38493.

PETROLOGY: Petrological descriptions, including microprobe data, of the rock are presented by McKay et al. (1973a,b) and Fruchter et al. (1974). Reed and Taylor (1974) discuss and provide metal compositions (lithology not stated) and MacDougall et al. (1973) report high-voltage electron microscope observations on dark materials. Wilshire and Moore (1974) depict the rock as a typical “black and white” breccia.

66055 consists of fragments of aphanitic dark materials and coarse light materials (Figs. 1 and 2). The dark materials vary from brown glass to mesostasis-rich basalt, with some fragments showing a gradation from one to the other (Fig. 2). The white fragments mainly have poikiloblastic (Fig. 2) or granoblastic textures while others are apparently cumulate (Fig. 2). Wilshire and Moore (1974) interpret the rock textures as indicating that dark material formed the original matrix to the rock and the white material was remobilized later; broken fragments of dark material have thin glassy selvages.

Fruchter et al. (1974), expanding on their previous work (McKay et al., 1973a) describe 66055 as containing clasts of brown glass, non-recrystallized breccia, partially-molten microbreccia (= basaltic impact melt), and anorthositic-noritic troctolitic (ANT) clasts. A feldspathic matrix is difficult to distinguish from the ANT clasts (They refer to the sample as a regolith breccia but regolith characteristics such as a wide variety of clasts including agglutinates are in fact absent). The brown glass contains plagioclase clasts (An₉₃₋₉₅). The non-recrystallized breccias (“equivalent to light and dark-matrix breccias”) contain pyroxene (Fig. 3), olivine, and plagioclase. The partially molten microbreccia is subophitic-ophitic. It contains clasts of plagioclase, olivine, and pyroxene in a medium-grained to cryptocrystalline matrix of plagioclase (An₉₃₋₉₅), olivine (Fo₇₅₋₈₂), and mesostasis. This lithology is distinctive for its metal blebs. The white clasts are anorthositic-noritic-troctolitic with textures ranging from primary igneous to cataclastic to poikiloblastic. Pyroxene compositions are shown in Figure 3. The matrix material described has fragments from 10 or 20 μm to 1 mm in diameter (the phrase “vast majority near 0.25 μm” in Fruchter et al. (1974) must be in error and probably should read 0.25 mm). Plagioclase, olivine, two pyroxenes, ilmenite, metal and troilite are present, with rare pink spinel.

McKay et al. (1973b) and to a lesser extent Fruchter et al. (1974) report kamacite-schreibersite compositions and relationships. Schreibersite is present most commonly in the subophitic melt but also occurs in the brown glass. Kamacite typically has ~4.4% Ni and ~0.4% Co. Experiments on melt compositional analogs produced an immiscible Fe-Ni-P liquid which crystallized to Fe-Ni metal and schreibersite. In the rock, the distribution of Ni between kamacite and schreibersite suggests that the particles last equilibrated at ~550°C. Reed and Taylor (1974) report metal compositions with 4-8% Ni, 0.2-0.5% Co, and up to 0.4% P, and note the presence of taenite.

MacDougall et al. (1973) report high-voltage electron microscope (HVEM) observations on the brown “glassy” lithology. The HVEM reveals that these in fact consist of packed agglomerations of submicron-sized crystallites which are severely deformed. A lack of solar flare tracks in the rock lead MacDougall et al. (1973) to conclude that 66055 is highly metamorphosed.

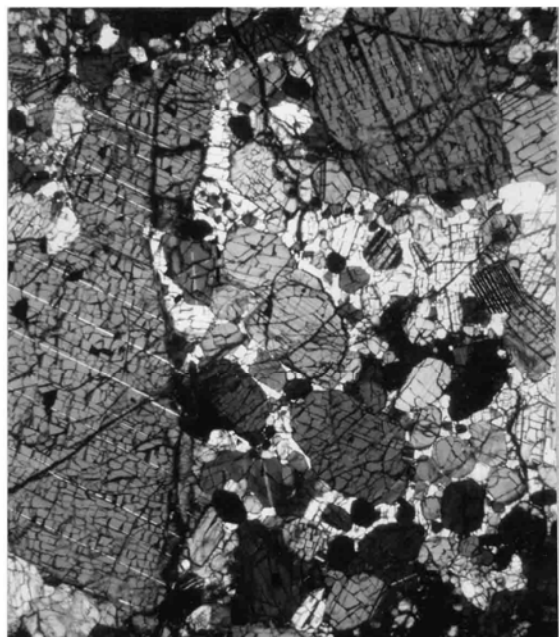
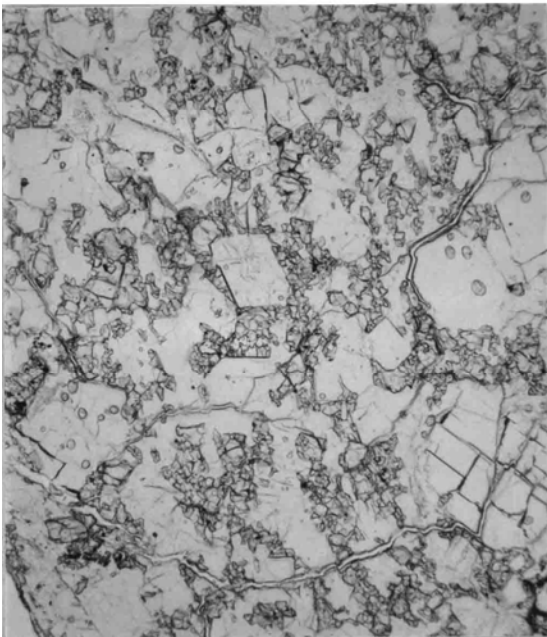
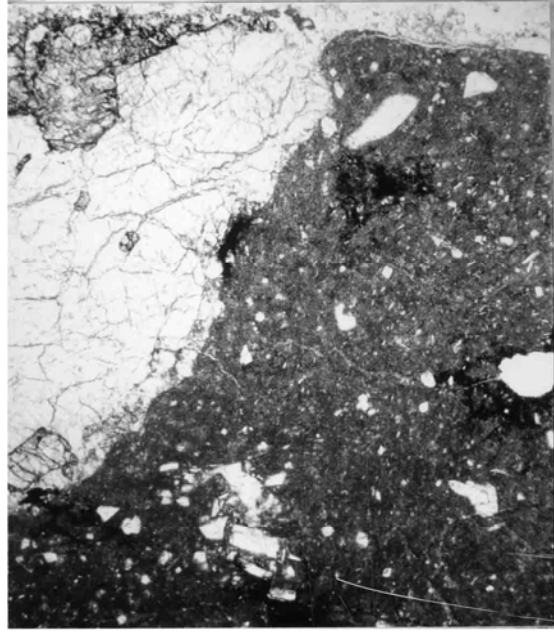
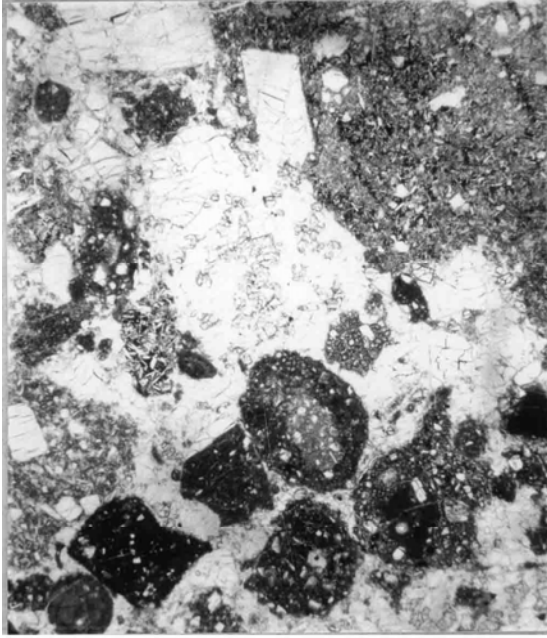


FIGURE 2.

- a) 66055,63. General view, ppl. Width 2 mm.
- b) 66055,71. General view, ppl. Width 2 mm.
- c) 66055,63. Poikiloblastic white material, ppl. Width 1 mm.
- d) 66055,75. Possible cumulate, xpl. Width 2 mm.

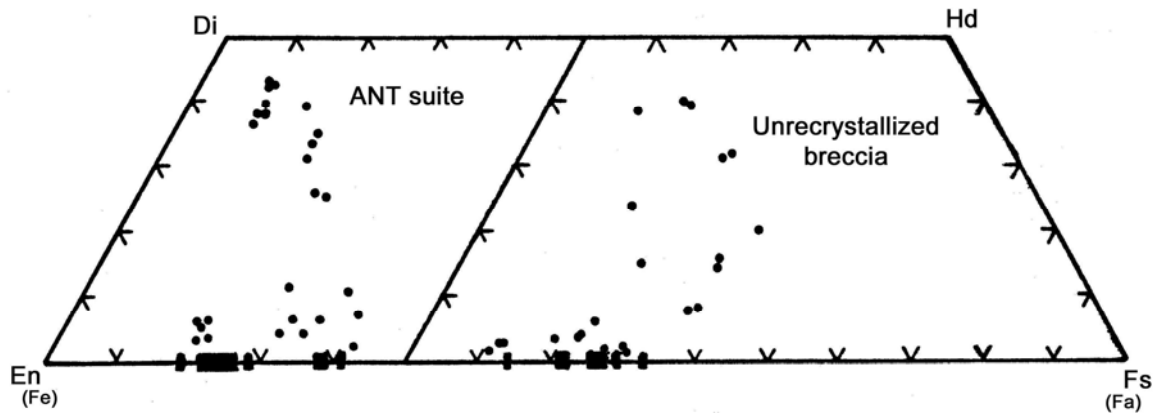


FIGURE 3. Mineral compositions, from Fruchter et al. (1974).

CHEMISTRY: Fruchter et al. (1974) report partial analyses, including trace elements, for matrix, and for white basaltic impact melt, unrecrystallized breccia, and unassigned clasts. They also report defocussed beam microprobe analyses of brown glass, unrecrystallized breccia, and basaltic impact melt fragments. S.R. Taylor et al. (1973) report a major and trace element analysis of white material (apparently white clasts and white matrix). The split number analyzed, reported as ,32, was in fact ,42. Moore et al. (1973), Cripe and Moore (1974) and Moore and Lewis (1976) report C, S (for white and mixed materials) and N (for white material) abundances respectively.

The data are summarized in Tables 1 and 2 and Figure 4. In general the distinction of white clast and matrix is difficult physically and the chemical ranges of these two are similar with an average of ~30% Al₂O₃. The brown glasses and unrecrystallized breccias are less aluminous than the basaltic impact melts, which appear to be similar to other aluminous melts among the Apollo 16 rocks. Nonetheless the range of compositions is not great. None of the materials are similar to local regolith although the average of the rock (light plus dark) *might* be. The low C abundances are not compatible with 66055 being a regolith breccia.

STABLE ISOTOPES: Clayton et al. (1973) report δO^{18} values for splits of 66055 (Table 3). These values are typical of lunar rocks.

GEOCHRONOLOGY: Phinney et al. (1975) report ⁴⁰Ar-³⁹Ar data for a mixed split of 66055. Its apparent age behavior (Fig. 5) is like that of Apollo 14 breccias. Because there is no unambiguous plateau, Phinney et al. (1975) calculate only a K-Ar age of 3.90 ± 0.02b.y. The data also imply that K and Ca are well-mixed in the sample. (Note that an explanation of the release pattern from recoil in fine-grained material is based on information from Fruchter et al. (1974) that most matrix grains are ~0.25 μm, which is probably erroneous).

TABLE 1. Summary chemical data for 66055 lithologies.

	<u>Light, a)</u> <u>matrix</u>	<u>Light, b)</u> <u>matrix</u>	<u>Subophitic c)</u> <u>melt</u>	<u>Unrex. c)</u> <u>breccia</u>	<u>White c)</u> <u>clasts</u>
SiO ₂	43.6				
TiO ₂	1.8*				
Al ₂ O ₃	31.4	29.4	23.7	25.9	27-36
Cr ₂ O ₃		0.10	0.16	0.11	0.003-0.14
FeO	2.2	4.4	8.5	5.4	0.1-4.3
MnO					
MgO	4.1				
CaO	16.8				
Na ₂ O	0.37	0.40	0.51	0.46	0.27-0.41
K ₂ O	0.10	0.11	0.25	0.22	<0.08
P ₂ O ₅					
Sr					
La	3.2	9.3	29.1	16.9	<3.7
Lu	0.14	0.55	1.3	0.85	
Rb	0.98				
Sc		6.5	11.9	8.7	0.4-6.5
Ni					
Co		25	62	32	1-22
Ir ppb					
Au ppb					
C		22			
N		49			
S		520			
Zn					
Cu					

Oxides in wt%; others in ppm except as noted.

a) S.R. Taylor et al. (1973)
b) Fruchter et al. (1974), and others
c) Fruchter et al. (1974)
* Possibly a typographical error; should be 0.18?

TABLE 2. Defocused beam microprobe analyses of 66055 lithic types (Fruchter et al., 1974).

<u>wt.%</u>	<u>brown glass</u>	<u>unrecrystallized breccia</u>	<u>basaltic impact melt</u>
SiO ₂	46.9	45.4	45.1
TiO ₂	1.2	1.1	0.9
Al ₂ O ₃	19.1	20.9	23.2
Cr ₂ O ₃	0.19	0.16	0.16
FeO	7.8	7.5	5.8
MgO	10.6	9.1	9.1
CaO	11.9	12.1	13.0
Na ₂ O	0.65	0.69	0.04*
K ₂ O	0.35	0.35	0.27
P ₂ O ₅	0.36	0.30	0.20

*probable typographical error; should be 0.4?

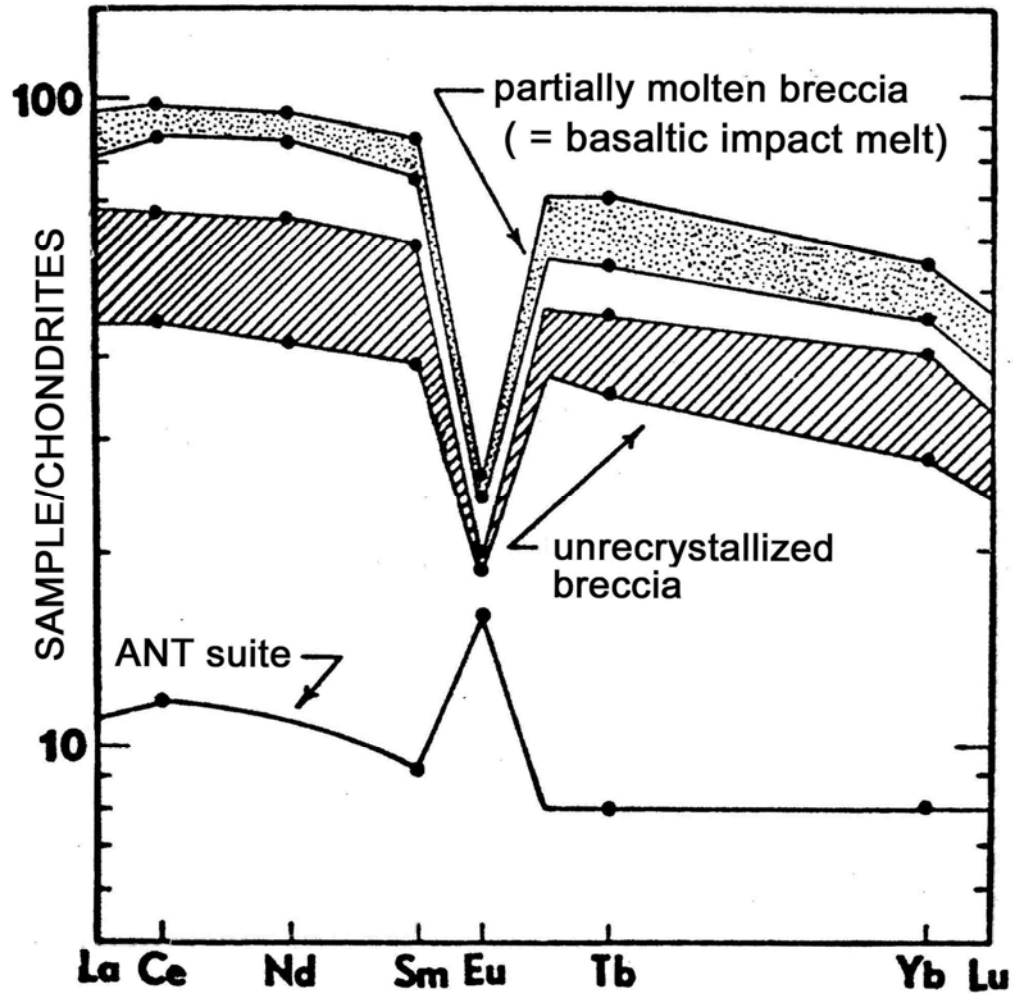


FIGURE 4. Rare earths, from Fruchter et al. (1974).

TABLE 3. δO^{18} for subdivisions of 66055,13.

whole rock	:+ 5.58 ‰
light clast	:+ 5.75 ‰
dark clast	:+ 5.48 ‰

EXPOSURE AGE: Phinney et al. (1975) report a ^{38}Ar -Ca exposure age of 55 ± 13 m.y. for a mixed split of 66055. MacDougall et al. (1973) found no solar flare tracks in the rock.

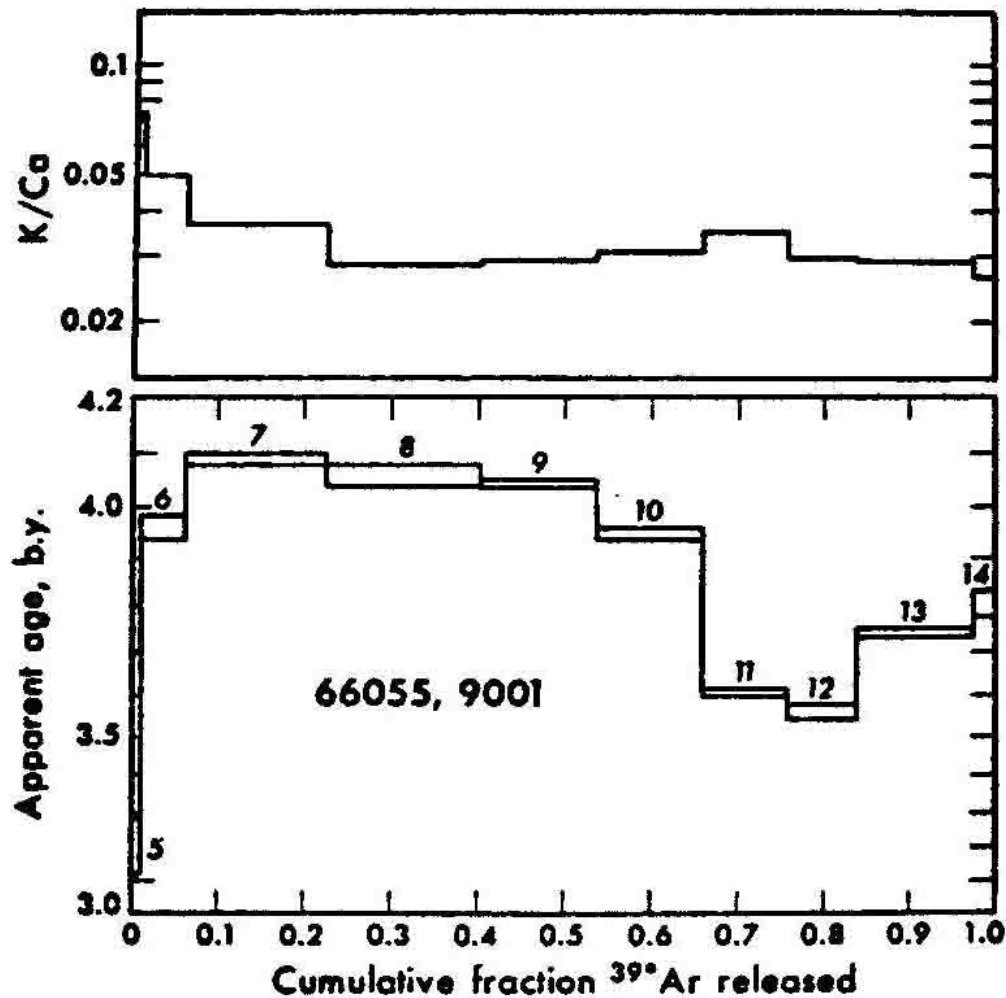


FIGURE 5. Ar releases, from Phinney et al. (1975).

PHYSICAL PROPERTIES: Collinson et al. (1973) report natural remanent magnetization (NRM) data for subsplits of a mixed sample. A chip had an NRM of $18.1 \times 10^{-6} \text{ emu} \cdot \text{g}^{-1}$, and after being split, the four subsplits had values of 30.0, 7.9, 7.3, and $15.6 \times 10^{-6} \text{ emu} \cdot \text{g}^{-1}$, i.e. quite variable. The variability showed no obvious correlation with the proportion of dark to light material. Figure 6 shows that the direction of NRM of the subsplits (A, B, F, R) are in reasonable agreement. A, F, and R had a dominantly soft NRM component; A had no detectable hard component at all. The *changes* in directions during demagnetization of the subsplits were different. A possible interpretation is that the breccia was not heated above the Curie point ($\sim 780^\circ\text{C}$) during formation and thus old hard components are preserved. *After* formation, a soft, stronger remanence of homogeneous direction was acquired. The variation in intensity could then be a result of variable iron contents of subsplits. Brecher (1975) interprets the inhomogeneity of NRM as supporting the model of "textural remanence."

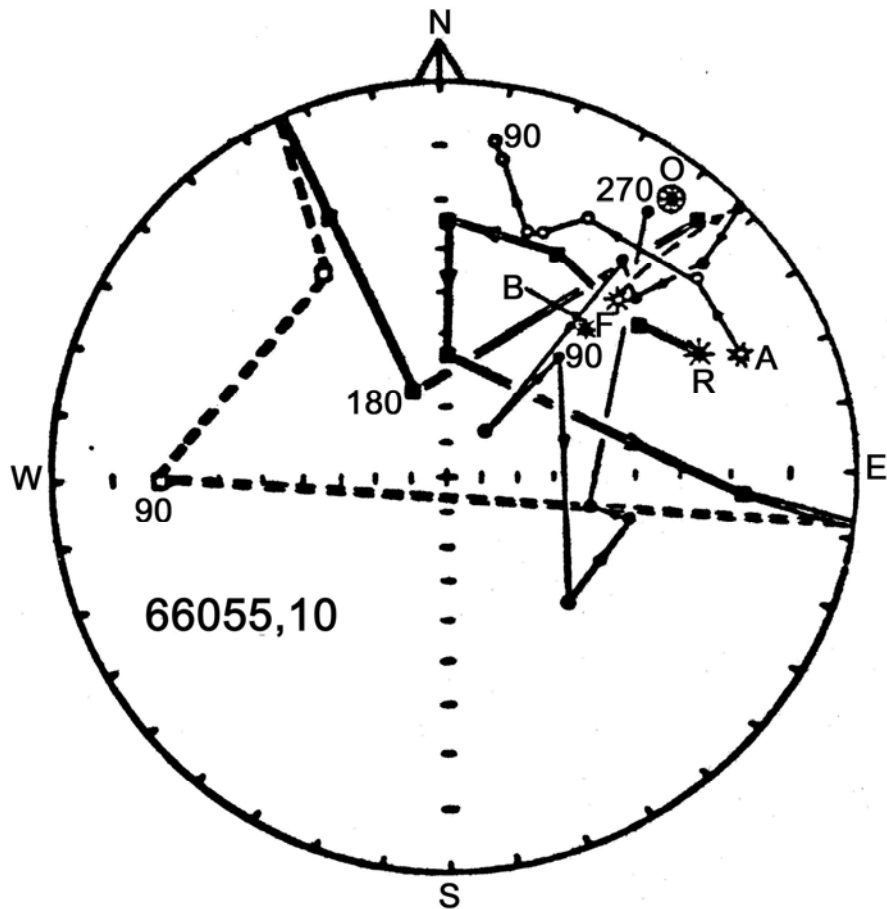


FIGURE 6. AF-demagnetization, from Collinson et al. (1973).

Nagata et al. (1973) tabulate basic magnetic properties for a mixed split and derive an average Ni content for kamacite of $6.0 \pm 0.5\%$ from magnetic methods. An extensive discussion of the intensity and stability of NRM is presented. Schwerer and Nagata (1976) use the previously reported magnetic data to obtain the size of the superparamagnetic iron particles (mean diameter of fine-grained particles = 54 \AA). They also summarize some of the magnetic properties relevant to the characterization of the superparamagnetic and ferromagnetic components. Schwerer et al. (1973) and Huffman et al. (1974) repeat some of the data of Nagata et al. (1973) but also report Mossbauer analyses for the distribution of Fe between phases, and the $\text{Fe}^0/\text{Fe}^{2+}$ ratio. The latter (0.045) is much lower than the value derived by magnetic measurements (0.205), a discrepancy typical of olivine-rich rocks and for which possible explanations are presented. 57.4% of the total Fe of the sample analyzed is in olivine, 37.8% in pyroxene, $\sim 0.5\%$ in ilmenite, and 4.3% in metallic iron.

Cisowski et al. (1974) plot Fe^0 of 0.4% (from their magnetic measurements) on an Fe^0 v. $\text{Fe}^0 + \text{Fe}^{2+}$ diagram. The determination is derived from the value of saturation magnetization, and assumes the metal to be entirely Fe^0 , neglecting other possible ferromagnetic phases.

Katsube and Collett (1973a) report electrical properties (Fig. 7) for a mixed chip which is mainly dark. The characteristics are unusual: in particular K (real relative permittivity) varies with frequency more than other lunar rocks and similarly to terrestrial pyroxenes and serpentines.

Warren and Trice (1975) illustrate the variations of dynamic modulus (from acoustic measurements), and static bulk modulus (from strain gauge measurements) with pressure. Apparently the sample used was a mixed dark and light chip.

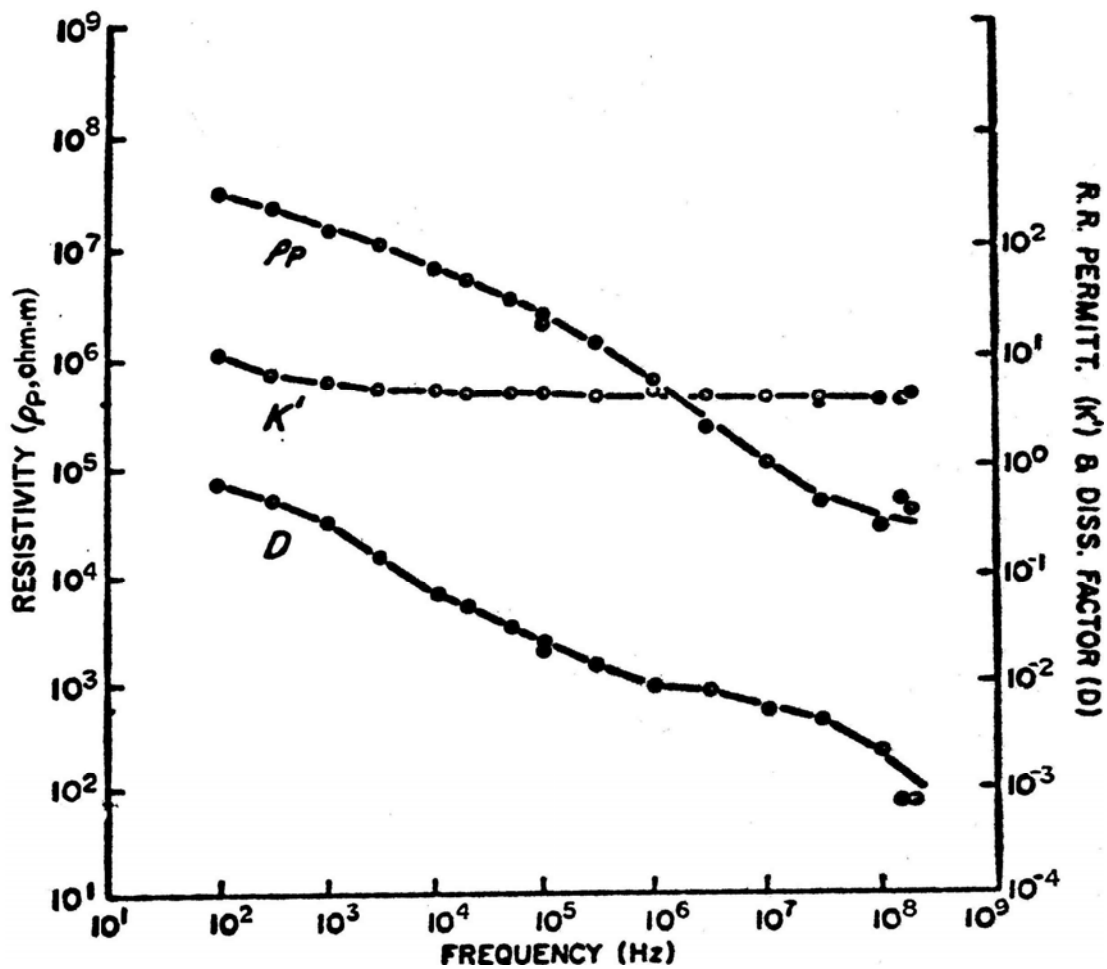


FIGURE 7. Electrical parameters. From Katsube and Collet (1973a).
 K' = real relative permittivity, P_p = parallel resistivity, D = dissipation factor.

PROCESSING AND SUBDIVISIONS: 66055 was sawn in 1972, producing two end pieces (.25; 231 g and .26; 673 g) and a slab piece (Fig. 8). The two end pieces remain intact except for a few small chips removed from .25. The slab has been extensively dissected (Fig. 9). A large split .24 (151 g) has broken into several pieces. More splits than are shown on Figures 8 and 9 have been made.

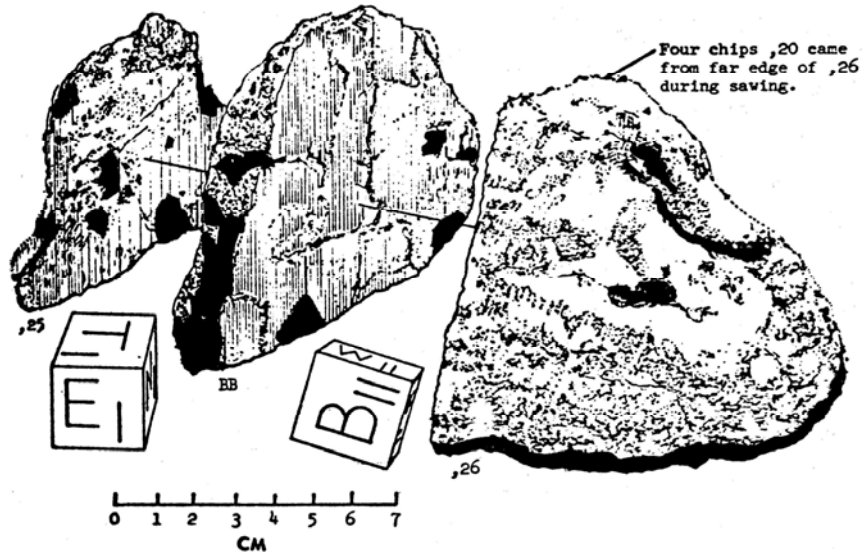


FIGURE 8. Cutting diagram.

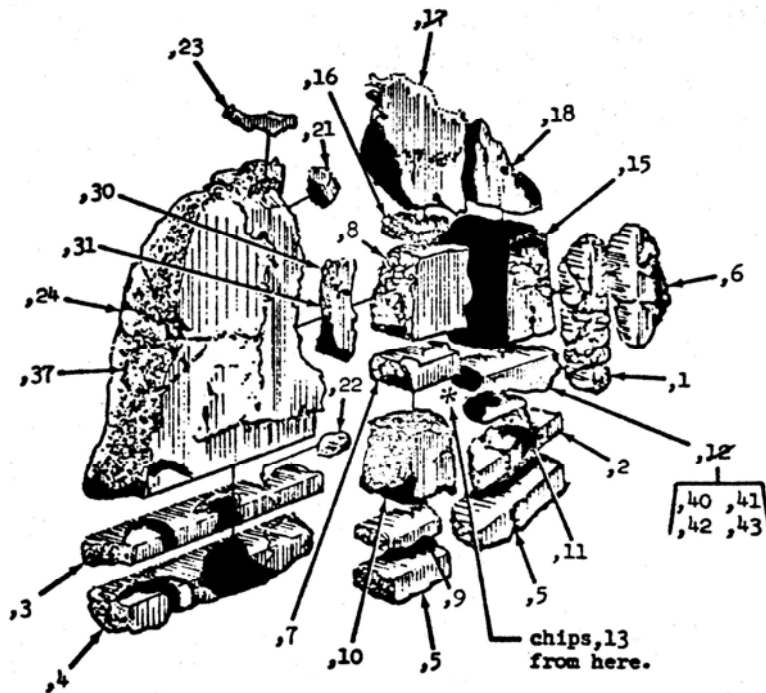


FIGURE 9. Slab subdivisions.